Drug Discovery

DOI: 10.1002/anie.201202544

Application of Fragment Screening and Merging to the Discovery of Inhibitors of the *Mycobacterium tuberculosis* Cytochrome P450 CYP121**

*Sean A. Hudson, Kirsty J. McLean, Sachin Surade, Yong-Qing Yang, David Leys, Alessio Ciulli, Andrew W. Munro, and Chris Abell**

The emergence of drug-resistant *Mycobacterium tuberculosis* (Mtb) drives a critical need for new front-line tuberculosis (TB) drugs with a novel mode of action.[1] It is estimated that there are over 650000 cases of multidrug-resistant tuberculosis emerging every year, and that 1.3 million cases will need to be treated by 2015, at a budgeted cost of over 16 billion US dollars.[2] The World Health Organization has declared this epidemic a global health emergency.[3]

The success of drugs that inhibit biosynthetic cytochrome P450 enzymes (CYPs), such as abiraterone, letrozole, and voriconazole, has propelled research towards understanding the unusually high number of CYPs (20) found encoded in the Mtb H37Rv genome.[4] Of particular interest is the essential CYP121 isoform, which has recently come into focus as an enticing new anti-TB drug target.[4a–c,5] This biosynthetic CYP appears to be exclusive to Mtb, and construction of an Mtb chromosomal *CYP121* knock-out mutant was only possible when a complementary vector carrying *CYP121* was present.[4b,5b] CYP121 has also recently been shown to catalyze an unusual intramolecular C–C bond-forming reaction between the *ortho*-positions of two tyrosines in cyclodityrosine (cYY) to form mycocyclosin.[5a] While the physiological roles of cYY and mycocyclosin remain to be determined, we believe that the unique catalytic action of CYP121 will lead to selective inhibitors. Specific inhibitors could also be used as chemical probes to show how this pivotal enzyme relates to Mtb infection, growth and persistence.

The only high-affinity ligands of CYP121 currently known are azole antifungals (traditional fungal CYP51 inhibitors, which act by way of type-II azole–heme coordination).[5b,6] These compounds exhibit potent in vitro/in vivo antimycobacterial activity, where their MIC (minimal inhibitory concentration) values for Mtb H37Rv correlate with their binding affinities to CYP121.[5b,7] However, the large flexible antifungals also have broad overlapping CYP inhibition profiles and are thus poor scaffolds for developing specific inhibitors and front-line TB drug candidates.[4a,6b,8] Those antifungals that are administered clinically, for example, fluconazole and voriconazole, also only bind weakly to CYP121.[5b,6a,8a] Furthermore, resistant Mtb mutants have already been isolated that show upregulation of a transmembrane transporter protein believed to act as an azole efflux pump.[9]

Fragment-based approaches represent a new method in the field of developing small-molecule ligands as chemical tools and leads for drug development.[10] This powerful method involves the structure-guided design and synthesis of potent ligands from weaker-binding low-molecular-weight fragment molecules (typically < 250 Da).[10] Herein, we report a fragment-based approach to targeting Mtb CYP121 in an attempt to identify new inhibitory molecules and to explore the active-site properties of the enzyme. Through an initial fragment-screening cascade involving thermal shift, NMR spectroscopy, and X-ray crystallography, four fragments were found to bind within the CYP121 active site, in two overlapping groups. A direct fragment–fragment merging strategy was implemented, leading to the discovery of a novel type-II aminoquinoline inhibitor with high ligand efficiency (LE $= -\Delta G$ of binding/non-hydrogen atoms (NHA) in the ligand) and fourfold greater affinity than the natural CYP121 substrate cYY. This lead provides a pattern for CYP121-specific inhibition and confirms the potential druggability of CYP121. This study represents the first successful application of fragment-based approaches to a cytochrome P450.

[*] S. A. Hudson, Dr. Y.-Q. Yang,[+] Dr. A. Ciulli, Prof. C. Abell
Department of Chemistry, University of Cambridge
Lensfield Road, Cambridge, CB2 1EW (UK)
E-mail: ca26@cam.ac.uk
Homepage: http://www-abell.ch.cam.ac.uk/

Dr. K. J. McLean, Prof. D. Leys, Prof. A. W. Munro
Manchester Interdisciplinary Biocentre, Faculty of Life Sciences, University of Manchester
131 Princess Street, Manchester, M1 7DN (UK)

Dr. S. Surade
Department of Biochemistry, University of Cambridge
80 Tennis Court Road, Cambridge, CB2 1GA (UK)

[+] Present address: Shanghai ChemPartner Co. Ltd.
Shanghai, 201203 (China)

[**] We acknowledge funding from the EC (as part of the NM4TB project) and the BBSRC (grants BB/I019227/1 and BB/I019669/1 to C.A. and A.W.M., respectively). S.A.H. was supported by a Sir Mark Oliphant Cambridge Australia Scholarship awarded by the Cambridge Commonwealth Trust & Cambridge Overseas Trust, University of Cambridge. We give thanks to: Dr. J. Goodman (Cambridge) for assisting with the in silico calculations; Dr. J. E. Davies (Cambridge) for determining the small molecule crystal structure of the 1,5-diphenoltriazole **7**; Dr. A. Boodhun (Cambridge) for performing mass spectrometry on recombinant His_6-tagged CYP121; Dr. C. Levy (Manchester) for help with synchrotron data collection; Prof. T. L. Blundell (Cambridge) for helpful discussions.

Supporting information for this article (experimental details) is available on the WWW under http://dx.doi.org/10.1002/anie.201202544. Crystal structures of the CYP121-ligand complexes are deposited in the Protein Data Bank (http://www.rcsb.org/pdb/) under the following accession codes: **1**: 4G44; **2**: 4G45; **3**: 4G46; **4**: 4G47; **7**: 4G2G; **10**: 4G48; **14**: 4G1X.

A rule-of-three-compliant library of 665 commercially available fragments (see Supporting Information) was initially screened for binding to recombinant CYP121 in a high-throughput 96-well plate format, using fluorescence-based thermal-shift analysis (Table 1 and Figure 1a). The melting point/denaturing temperature (T_m) of CYP121 alone (10 μM) was 50.1 ± 0.1 °C ($n = 20$), and cYY used as a control (1 mM) gave a ΔT_m of 1.0 ± 0.1 °C ($n = 6$). Fragment hits were defined as those that increased the melting point (ΔT_m) by more than 0.8 °C at a concentration of 5 mM; 66 hits were identified in total (9.9% hit rate).

Table 1: Fragment-screening statistics.

	No. of compounds	Hit rate[a] [%]
Fragments screened by thermal shift	665	
Thermal shift hits ($\Delta T_m > 0.8$ °C)	66	9.9
Fragments rescreened by 1D ^{1}H NMR	56	
cYY-displaced NMR hits	26	3.9

[a] Hit rate as a percentage of the total fragments screened.

Fifty-six of the most chemically diverse hits from the thermal shift screen were then screened by ligand-detected 1D ^{1}H NMR spectroscopy using saturation transfer difference (STD) and WaterLOGSY experiments (Table 1 and Figure 1b). Of these hits, 26 showed prominent interactions with CYP121 and were partially displaced by the addition of cYY (46% validated hit rate), indicating that they may bind within the active site. The solubility of the displaced NMR hits was then tested in the mother liquor used for CYP121 crystallization at 1 mM, and eight fragments showing the greatest solubility were studied by protein X-ray crystallography. We also conducted an identical fragment screen in parallel against a second Mtb CYP, the CYP125 cholesterol/cholestenone carbon-27 monooxygenase, which gave nine hits in total.[16] There was only a single hit common to both CYPs, indicating a surprisingly high degree of isoform selectivity even at the fragment-screening level.

CYP121 crystals were individually soaked with each of the eight most soluble NMR-validated hits, leading to the determination of four structures of CYP121 bound to fragments at 1.24–1.53 Å (Figure 2, see Figure S2 in the Supporting Information for the soaked fragments that did not yield fragment-bound structures). All of the fragments (**1**–**4**) bound within the large water-filled CYP121 distal active site (Figure 2b), and a superimposition of the structures reveals that the fragments form two overlapping groups that occupy a near continuous stretch between the heme iron and the top of the active site cavity (Figure 2c). Their overlapping binding modes also define the proposed CYP121 substrate entry channel/trajectory,[11] and provide a clear possibility for synthetic elaboration by fragment merging. There is no significant change in CYP121 conformation upon binding of the fragments compared to the native structure (C_α RMSD = 0.12–0.14 Å).[11]

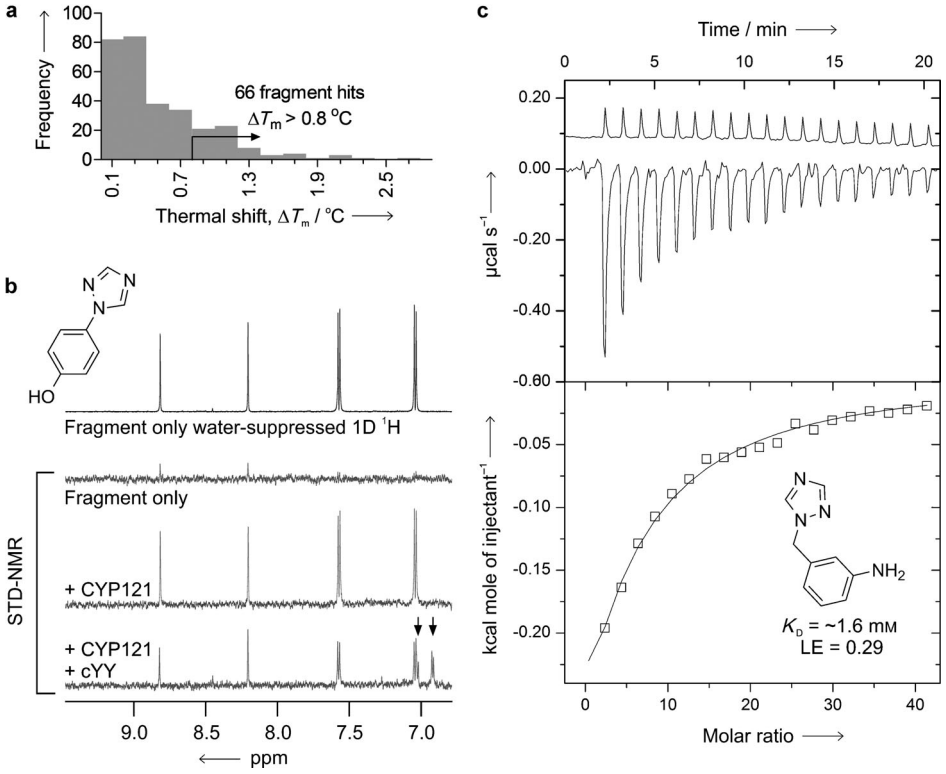

Figure 1. Fragment screening by thermal shift, NMR spectroscopy, and ITC. a) Histogram of fragments found to increase the melting point of CYP121 (10 μM) by fluorescence-based thermal-shift assay. Fragments were present at 5 mM and CYP121 thermal denaturation was monitored by SYPRO Orange (2.5×) fluorescence emission intensity. b) Water-suppressed 1D ^{1}H and STD NMR spectra for a representative fragment hit (1.5 mM) in the presence and absence of CYP121 (15 μM) or CYP121 (15 μM) plus cYY (0.5 mM). Only the fragment resonances in the aromatic region are shown and arrows indicate the signals from cYY. The strong positive fragment signals in the presence of CYP121 indicate protein binding, and this interaction is displaced/reduced by the addition of cYY. c) ITC binding isotherm for a representative fragment hit (20 mM) titrated into CYP121 (100 μM; lower trace) or buffer only (upper trace) as a negative control. The integrated enthalpy change for each injection as a function of the molar ratio of total injected ligand to CYP121 is shown (squares), with the one-site binding model fitted for estimating the K_D (line).

Fragments **1** and **2** coordinate the heme iron through their arylamine nitrogen in the sixth distal ligand position (Figure 2b). This type-II binding mode has not been reported before for CYP121. However a similar mode of coordination has been observed for arylamines binding to the orphan Mtb CYP130.[12] One of the amine protons is involved in hydrogen bonding (H-bonding) to the adjacent CYP121 Ser237. The aromatic

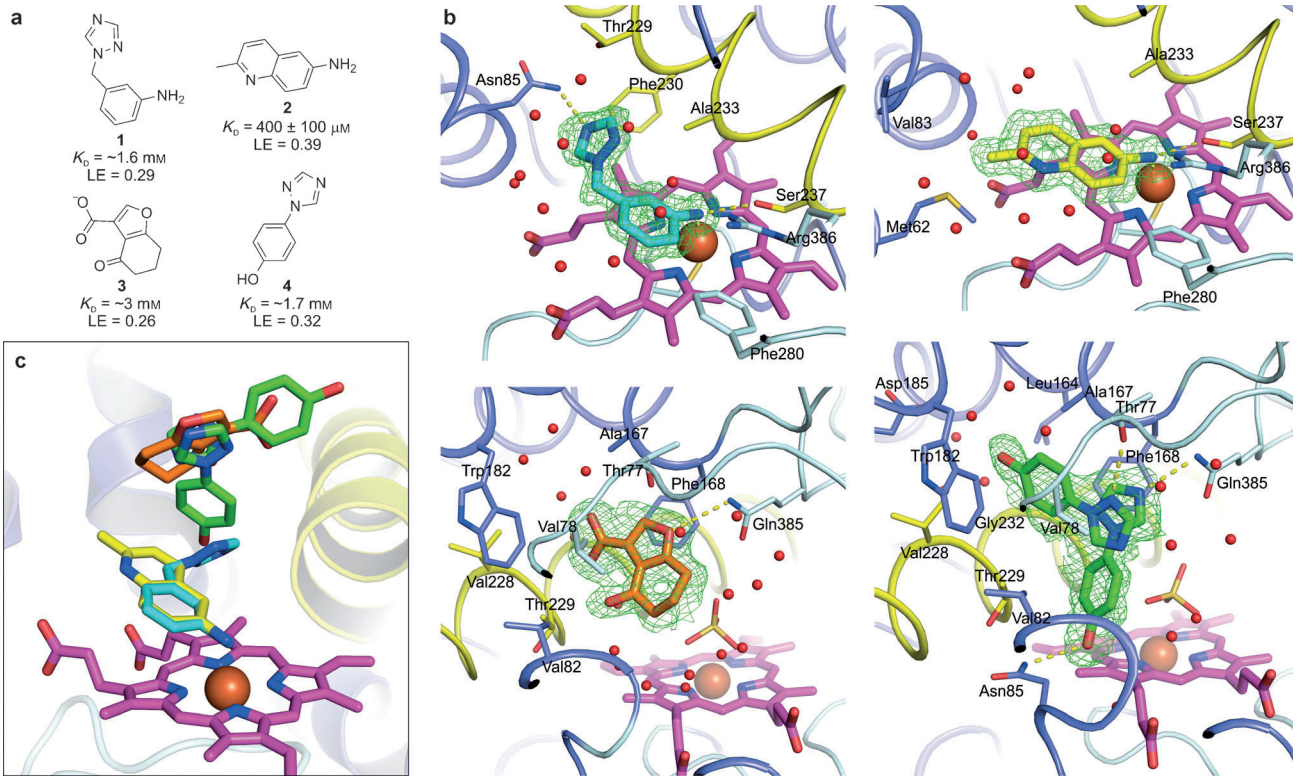

Figure 2. 1.24–1.53 Å resolution X-ray crystal structures of fragment hits **1**–**4** binding to CYP121. a) Fragment hit chemical formulas drawn in their predominant protonation state at pH 5-6 (CYP121 crystallization pH) and their associated K_D values and calculated LEs (kcal mol^{-1} NHA^{-1}), determined by ITC. b) Fragments **1**–**4**: thick sticks; heme *b*: purple; heme iron: brown sphere; I-helix: yellow; side chains/sulfates and waters (within 5 Å of the bound fragments): thin sticks and red spheres, respectively; direct fragment–CYP121 H-bonds and fragment–heme iron coordination: dashed yellow lines. The F_o-F_c omit electron density map associated with each fragment is shown as a green mesh contoured at 3σ. c) Overlay of fragments **1**–**4** within the active site from the crystal structures. The large 1350 Å^3 active site cavity is bent around the I-helix (yellow) that runs closely above the heme.

moieties of both fragments occupy a near parallel position to the heme, suggesting possible aromatic-stacking effects with the protoporphyrin IX. The quinoline nitrogen of fragment **2** also forms a water-mediated interaction with a heme carboxylate. The 1,2,4-triazole of fragment **1** is modeled with the nitrogen in the 4-position H-bonding directly to Asn85, based on structure-activity relationships (SARs; see below).

Fragments **3** and **4** reside further from the heme coordination sphere, with their five-membered aromatic rings in an offset π-stack with Phe168 (Figure 2b). Only the furan oxygen of **3** appears to make a direct H-bond with CYP121 through Gln385. Fragment **4** lies in two configurations centered around its triazole (each modeled at half occupancy). In one configuration the phenol forms an H-bond with Asn85, and in the other the phenol stacks between Phe168 and Trp182. Its triazole 2- and 4-position nitrogen atoms may H-bond to either Thr77 or Gln385.

It is interesting that the azole moiety in two of the fragments (**1** and **4**) does not coordinate the heme iron (Figure 2b), as is typically observed for the azole antifungal CYP inhibitors.[13] We have seen the same thing for CYP121 binding by the antifungal fluconazole, where indirect coordination of an interstitial water is the dominant binding mode in the crystal structure.[14] Our hypothesis is that orthogonal heme coordination by *N*-heterocycles is disfavored in CYP121 because of the unusually close I-helix residues above the heme.

The CYP121-binding affinity of fragments **1**–**4** (equilibrium dissociation constants, K_D) and calculated LEs (Figure 2a), were determined by isothermal titration calorimetry (ITC) using direct titrations of the fragment into a solution of CYP121 (see Figure 1c for example) or, when large heats of dilution obscured the signal, by a competitive ITC experiment titrating cYY into a solution of CYP121 pre-mixed with the fragment. These fragments have K_D values from 400 μM to 3 mM. The highest-affinity heme-coordinating fragment **2** has a corresponding LE of 0.39 kcal mol^{-1} NHA^{-1}. Interestingly, the weakest-binding fragment **3** is also the one appearing to make only a single direct H-bond with CYP121.

To increase the binding affinity of fragments **1**–**4** through merging, several merged fragments and their structural analogues were synthesized or obtained commercially (Figure 3 and Supporting Information; Figure S3). Their binding affinities (Figure 3) were determined by either ITC as described above, or for the heme-coordinating aminoquinolines **14**–**19**, by a spectrophotometric assay monitoring type-II red shifts in the heme absorbance band.

Merging the weaker fragments from the upper region of the active site (**3** and **4**, or the two configurations of **4** alone) to form compounds **5**–**11** did not lead to significantly higher

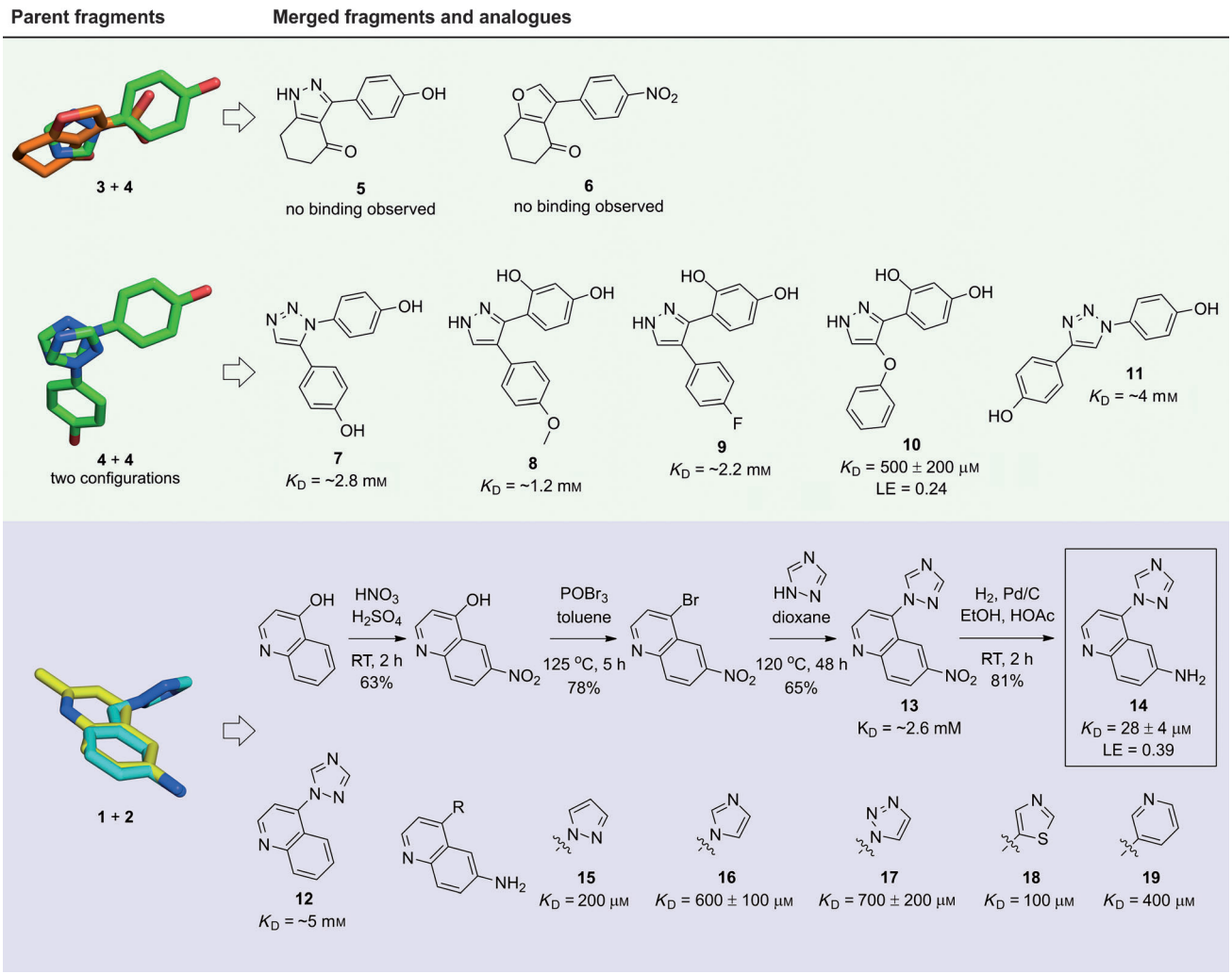

Figure 3. Binding affinity and SAR of merged fragments and analogues. The parent fragment pairs (from Figure 2c) from which the merged fragments were derived are shown as thick sticks. K_D and LE values (kcal mol^{-1} NHA^{-1}) were determined by ITC or, for **14**–**19**, by spectrophotometric heme-absorbance shift assay. Single determinations are rounded to the nearest 100 μM and repeat measurements are given as the mean ± s.e.m. (n = 3 or 4). Compound formulas are drawn in their predominant protonation state at pH 7.4. Synthesis of **14** is shown; the syntheses of other analogues are shown in the Supporting Information, Figure S3.

affinity (Figure 3). The cyclohexanone-containing analogues **5** and **6** gave no ITC binding isotherms and were not competitive with cYY in the NMR binding assays. This loss of binding may be because of the relatively poor superposition of fragments **3** and **4**, or the loss of binding interactions from replacing the carboxylate of **3** with the phenol of **4**. The biaryl-substituted azoles **7**–**9** show binding, but with no significant improvement over their parent fragment **4**. In an attempt to understand the poor binding of **7**–**9**, we performed quantum mechanical (QM) calculations for the conformational energetics of **7** (Supporting Information, Figure S4). These calculations suggest that a binding position identical to fragment **4** (Figure 2b) would be strained, with the *ortho* hydrogen atoms of **7** on opposite phenol groups pointing/clashing towards each other. A small-molecule crystal structure of **7** alone however shows crystal packing in a conformation near the calculated energetic minima (Supporting Information, Figure S4). Based on these findings, we propose that the weak affinity of **7**–**9** could be the result of a high conformational energy barrier necessary for binding to CYP121. Moreover, the best compound of the weak series **5**–**11**, the phenoxypyrazole **10** (K_D = 500 ± 200 μM), potentially avoids such internal strain owing to the oxygen separating its phenoxy and pyrazole rings.

Compounds **12**–**19**, based on merging the two heme-ligating fragments **1** and **2**, proved significantly more successful (Figure 3). All type-II-binding aminoquinolines **14**–**19** show improved affinity over their constituent azole fragment **1**. The lead compound in the series is the 1,2,4-triazolylquinoline **14** (Figure 3, boxed), which retains the original 1,2,4-triazole subunit of fragment **1**, has a K_D of 28 ± 4 μM (n = 4; using both methods of affinity determination; see Figure 4b), and high LE (0.39 kcal mol^{-1} NHA^{-1}), equal to that of its root fragments. Significantly, **14** has fourfold greater affinity than the natural substrate cYY (K_D = 110 ± 12 μM by ITC, n = 7,[5a] K_D = 21.3 ± 3.5 μM by spectral titrations) and inhibits CYP121

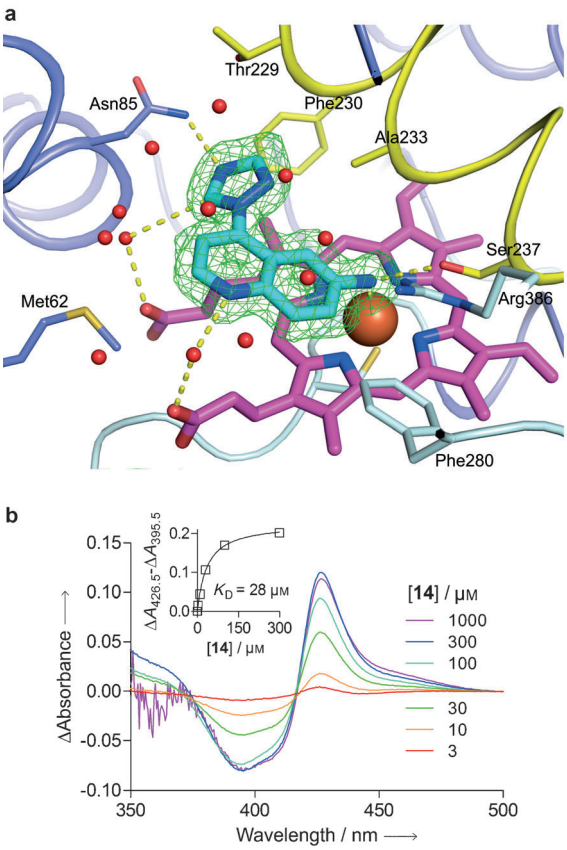

Figure 4. Novel type-II binding to CYP121 by **14**. a) The CYP121 active-site complex with **14** (cyan) from a 1.30 Å crystal structure. View and colors are the same as those described in Figure 2b. b) Absorbance difference spectra for CYP121 (5 μM) titrated with various concentrations of **14**. The red shift in the heme Soret absorbance band induced by **14** (shown as a ΔA_{max} at 426.5 nm and ΔA_{min} at 395.5 nm in the difference spectra) is indicative of inhibitory type-II CYP binding associated with heme-iron coordination.[13] Inset: the change in heme absorbance (quantified as $\Delta A_{max}-\Delta A_{min}$) as a function of **14** concentration (squares) with the one-site binding equilibrium model fitted for calculating the K_D (line).

catalytic activity with a K_i of 50 μM in a coupled-absorbance enzyme assay with heterologous redox partners. **14** also shows no affinity for Mtb CYP125 by ITC (data not shown), consistent with the isoform specificity observed in the fragment screens, and has weak to no inhibitory effect on several major metabolizing human hepatic CYPs (IC_{50} for CYP2C19 > 100 μM; 2D6 > 100 μM; 3A4 > 100 μM (probe substrate testosterone); 3A4 = 65 μM (probe substrate midazolam)).

The analogues of lead **14** synthesized in the series **12**–**19** shed light on its SAR (Figure 3). Removal of the heme-coordinating amino group from **14** (see **13**) or its nitro precursor (see **12**) resulted in over 90-fold weaker affinity. This gives the amine a group efficiency of 2.6 kcal mol^{-1} NHA^{-1} (GE = $-\Delta\Delta G$ of binding/ΔNHA), clearly indicating the critical strength of the heme-coordinating interaction. Analogues **15**–**19** were developed to explore binding within the azole pocket along the I-helix defined by fragment **1** (assuming they all bind to CYP121 in the same position as **1**) and were synthesized based on the strategy used for **14**. Replacing the 2- or 4-position triazole nitrogen atoms of **14** with C–H in the pyrazolyl-, imidazolyl- and 1,2,3-triazolyl analogues **15**–**17** was not well tolerated. The larger ring sizes of the thiazole or pyridine in **18** and **19** were also not accommodated. These SAR data indicate that the 1,2,4-triazole in fragment **1** and lead **14** may be optimal for the CYP121 pocket defined by Asn85, Thr229, and Ala233, because its 4-position nitrogen atom H-bonds to Asn85, and its 2-position nitrogen atom (over C–H) removes a steric clash with Ala233. We have modeled the fragment **1**–CYP121 structure accordingly (Figure 2b). The methyl from fragment **2** was intentionally excluded from analogues **12**–**19** for ease of synthesis and because it appeared to point unfavorably into the CYP121 water-filled pocket around the heme carboxylates (Figure 2b). The analogue of fragment **2** without the methyl group, 6-aminoquinoline (not included in the initial fragment screen), was also tested and has a similar K_D of 300 μM by ITC.

X-ray crystal structures of **7**, **10**, and **14** in complex with CYP121 were obtained at 2.25, 1.50 and 1.30 Å resolution, respectively, showing that all three ligands adopt the binding mode of their parent fragments (Figure 4a and Supporting Information, Figure S5; compared to Figure 2b). Both the weak 1,5-diphenoltriazole **7** and its higher affinity phenoxypyrazole analogue **10** reside in the position distant from the heme, like the two orientations of fragment **4**. The phenol pair of **7** appears to be sandwiched in the conformationally strained state predicted by QM calculations (Supporting Information, Figure S4c), that is, with its *ortho* hydrogen atoms on opposite phenols pointing into each other to one side of the triazole ring. The phenoxy sp^3 oxygen atom of **10** clearly alleviates a clash of *ortho* hydrogen atoms by adding a bond between the phenoxy and pyrazole rings, and also allowing the phenoxy ring to twist out of the pyrazole plane. Taken together, these findings form a pertinent illustration of the importance of considering the conformational freedom of elaborated fragments made using fragment-based approaches. It is worth noting that the *ortho*-hydroxy group and pyrazole nitrogen atom (or N–H tautomer) of **10** find a double H-bond interaction with Thr77, which may add to its improved affinity over **7**.

The lead aminoquinoline **14** coordinates the heme iron through its arylamine nitrogen atom (not the azole) face-on in the distal coordination site, identical to fragments **1** and **2** (Figure 4a compared to Figure 2b). The orientation of Asn85 and its 1,2,4-triazole has been modeled to match the SAR of the aminoquinoline analogues **14**–**19** discussed above. This places the acidic triazole 5-position C–H group of **14** in-line to form a second water-bridged H-bond with a heme carboxylate. QM calculations for this CYP121-bound pose of **14** and also the phenoxypyrazole **10** indicate no significant internal strain relative to their predicted ground-state conformation in the gas phase (data not shown).

This study represents the first fragment-based approach to targeting a biosynthetic cytochrome P450. The findings are also the first significant advance towards the rational design of any Mtb CYP inhibitor and CYP-targeting TB drug candidate. The binding modes of the developed ligands have given

us unique insights into the active site properties of CYP121. We were particularly fortunate to find fragments having the correct overlapping binding poses to study using direct fragment–fragment merging. This is not common in fragment-based drug discovery, and usually hybrid merged molecules are developed by combining fragment hits with elements from a larger known substrate, cofactor, or inhibitor.[15] Our novel lead **14**, with its high LE and selectivity, provides an excellent scaffold for further type-II, reversible, competitive CYP121 inhibitors. Linking **14** with the non-heme coordinating fragments **3** and **4** presents an attractive way forward, and we have begun assessing the anti-tubercular efficacy of compounds developed in this series. The findings lay the groundwork for the deployment of fragment-based design to other members of the cytochrome P450 superfamily. Characterization of fragment-binding modes to orphan CYPs may even shed light on their likely functions at the substrate level. For instance, it is intriguing that the CYP121 natural substrate cYY is a biphenol and we also find the phenol fragment **4** bound in two configurations (Figure 2b).

Received: April 1, 2012
Revised: June 10, 2012
Published online: August 13, 2012

Keywords: cytochrome P450 · drug design · fragment screening · tuberculosis

[1] A. Koul, E. Arnoult, N. Lounis, J. Guillemont, K. Andries, *Nature* **2011**, *469*, 483.
[2] a) World Health Organization, 2011/2012 Tuberculosis Global Facts, **2011**; b) World Health Organization, Multidrug and extensively drug-resistant TB (M/XDR-TB): 2010 global report on surveillance and response, **2010**.
[3] World Health Organization, Global tuberculosis control: WHO report 2011, **2011**.
[4] a) S. A. Hudson, K. J. McLean, A. W. Munro, C. Abell, *Biochem. Soc. Trans.* **2012**, *40*, 573; b) H. Ouellet, J. B. Johnston, P. R. Ortiz de Montellano, *Arch. Biochem. Biophys.* **2010**, *493*, 82; c) K. J. McLean, J. Belcher, M. D. Driscoll, C. C. Fernandez, D. Le Van, S. Bui, M. Golovanova, A. W. Munro, *Future Med. Chem.* **2010**, *2*, 1339; d) S. T. Cole, et al., *Nature* **1998**, *393*, 537.
[5] a) P. Belin, et al., *Proc. Natl. Acad. Sci. USA* **2009**, *106*, 7426; b) K. J. McLean, et al., *J. Biol. Chem.* **2008**, *283*, 33406.
[6] a) K. J. McLean, et al., *J. Inorg. Biochem.* **2002**, *91*, 527; b) F. C. Odds, A. J. Brown, N. A. Gow, *Trends Microbiol.* **2003**, *11*, 272.
[7] a) S. T. Byrne, S. M. Denkin, P. Gu, E. Nuermberger, Y. Zhang, *J. Med. Microbiol.* **2007**, *56*, 1047; b) Z. Ahmad, S. Sharma, G. K. Khuller, *FEMS Microbiol. Lett.* **2006**, *258*, 200; c) Z. Ahmad, S. Sharma, G. K. Khuller, *FEMS Microbiol. Lett.* **2005**, *251*, 19.
[8] a) J. R. Perea, B. S. Diaz De Rada, E. G. Quetglas, M. J. Juarez, *Clin. Microbiol. Infect.* **2004**, *10 Suppl 1*, 96; b) J. A. Como, W. E. Dismukes, *N. Engl. J. Med.* **1994**, *330*, 263.
[9] A. Milano, M. R. Pasca, R. Provvedi, A. P. Lucarelli, G. Manina, A. L. Ribeiro, R. Manganelli, G. Riccardi, *Tuberculosis* **2009**, *89*, 84.
[10] a) D. E. Scott, A. G. Coyne, S. A. Hudson, C. Abell, *Biochemistry* **2012**, *51*, 4990; b) C. W. Murray, M. L. Verdonk, D. C. Rees, *Trends Pharmacol. Sci.* **2012**, *33*, 224; c) "Fragment-Based Drug Discovery and X-Ray Crystallography": *Topics in Current Chemistry*, *Vol. 317* (Eds.: T. G. Davies, M. Hyvönen), Springer, Heidelberg, **2012**.
[11] D. Leys, C. G. Mowat, K. J. McLean, A. Richmond, S. K. Chapman, M. D. Walkinshaw, A. W. Munro, *J. Biol. Chem.* **2003**, *278*, 5141.
[12] L. M. Podust, H. Ouellet, J. P. von Kries, P. R. Ortiz de Montellano, *J. Biol. Chem.* **2009**, *284*, 25211.
[13] P. R. Ortiz de Montellano, *Cytochrome P450: Structure, Mechanism, and Biochemistry*, 3rd ed., Kluwer Academic/Plenum Publishers, New York, **2005**.
[14] H. E. Seward, A. Roujeinikova, K. J. McLean, A. W. Munro, D. Leys, *J. Biol. Chem.* **2006**, *281*, 39437.
[15] a) D. A. Erlanson, R. S. McDowell, T. O'Brien, *J. Med. Chem.* **2004**, *47*, 3463; b) E. Edink, et al., *J. Am. Chem. Soc.* **2011**, *133*, 5363.
[16] S. A. Hudson, et al., unpublished results.

